THE ASTROPHYSICAL JOURNAL, 221:137–144, 1978 April 1

ACCURATE INTERFEROMETER POSITIONS OF H_2O MASERS

J. R. FORSTER, W. J. WELCH, AND M. C. H. WRIGHT
Radio Astronomy Laboratory, University of California, Berkeley
AND
A. BAUDRY
Observatoire de l'Université de Bordeaux, France
Received 1977 September 7; accepted 1977 October 5

ABSTRACT

We report accurate interferometer positions for strong water-vapor masers in the regions ON 1, W51, VY CMa, Sgr B2, W75, and NGC 7538. The absolute position uncertainties are mostly less than $\sim 0''.5$. Among the 13 H_2O maser sources or groups of spots for which accurate interferometer positions are available, no infrared point sources are coincident in eight cases, OH masers may be coincident in six cases, and H_2O masers lie at the edge of compact H II regions in five cases. In four out of the latter five cases, no infrared emission is seen toward the compact H II regions. Thus the maser emission does not arise in a dense shell of dust, a cocoon that completely surrounds the O star and its compact H II region, because such a shell would have a large infrared luminosity. It appears, rather, that the maser emission arises in separate fragments or condensations.

Subject headings: infrared: sources — interferometry — interstellar: molecules — masers — radio sources: general

I. INTRODUCTION

The absolute position is one of the most important parameters in understanding the H_2O maser sources both in their internal mechanics and in their role in star-formation regions. To this end, a continuing program of accurate position measurements has been undertaken with the Hat Creek interferometer described in detail by Welch *et al.* (1977). The present set of measurements were made in 1975 November through 1976 February and in 1976 November for the sources ON 1, ON 2, W51, VY CMa, Orion, Sgr B2, W75, and NGC 7538. The results for the W3 region, CRL 2591, and W49 appear elsewhere (Forster, Welch, and Wright 1977; Wynn-Williams *et al.* 1977; Dieter, Welch, and Wright 1978).

II. OBSERVATIONS AND DATA REDUCTION

The observations were made with the Hat Creek interferometer, which consists of two 6 m antennas allowing for maximum separations of 300 m east-west and 200 m north-south; 300 m provides a minimum lobe spacing of 8″ at 1.35 cm. The strong H_2O sources discussed here exhibit point source visibilities, and only a few interferometer spacings were used for the observations. The filter bank of the interferometer has 128 channels with either 250 kHz or 15 kHz filters, providing a resolution of either 3 km s^{-1} or 0.2 km s^{-1} at 1.35 cm wavelength.

The positions of the H_2O maser sources are found relative to nearby quasars whose positions are known to better than $0''.1$ (Elsmore and Ryle 1976). Since both are effectively point sources, we need consider only the phases of the fringes produced by either source. The difference between the observed and expected fringe phase for a source of nominal baseline components (b_1, b_2, b_3) is given by

$$\Delta\phi = \frac{2\pi}{\lambda}\,[\Delta b_1 \cos\delta\cos h - \Delta b_2 \cos\delta \sin h + \Delta b_3 \sin\delta + (-b_1 \cos\delta \sin h - b_2 \cos\delta \cos h)\Delta h + (-b_1 \sin\delta \cos h + b_2 \sin\delta \sin h + b_3 \cos\delta)\Delta\delta]\,, \quad (1)$$

where Δh and $\Delta\delta$ are the differences between the true and nominal coordinates; Δb_1, Δb_2, and Δb_3 are differences between the true and nominal baseline components; and λ is the wavelength. At any particular arrangement of the two antennas, the preliminary baseline components are first obtained by conventional survey techniques to an accuracy of about 1 cm. Then the H_2O maser position determination requires two further steps: (1) accurate baseline calibration based on quasar positions, and (2) the unknown source observations.

For the accurate baseline calibration, several quasars are observed at a wide range of hour angles. For these $(\Delta h, \Delta\delta) = 0$ in equation (1); and Δb_1, Δb_2, and Δb_3 are found by a least-squares fit of equation (1) to the quasar phases. The probable error in this determination is typically 0.3 mm for the present observations.

The second part of the maser position determination is the observation of the maser fringe phase and the

determination of Δh and $\Delta\delta$ from equation (1). Two different techniques were used for all the sources studied. In the first technique, each source was tracked over the available hour angle, with the antennas arranged to provide a long east-west baseline. The resulting phase as a function of h was then fitted to equation (1), with the correct baseline ($\Delta b_1 = \Delta b_2 = \Delta b_3 = 0$), by using the method of least squares to find Δh and $\Delta\delta$. In the second technique, the sources were observed only near meridian transit, and the difference between the unknown source phase and that of a nearby quasar was used to find Δh and $\Delta\delta$ from equation (1). An east-west baseline gives essentially Δh, and a north-south baseline gives essentially $\Delta\delta$. Instrumental errors affect the methods differently and are discussed in the following subsection.

a) Tracking Sources over Large Hour Angles

Following a point source for many hours gives a large number of independent data. A least-squares fit of equation (1) to the data then gives Δh and $\Delta\delta$ with small formal errors (when one considers the signal-to-noise ratio in the present observations). The long run also eliminates lobe ambiguities. However, over several hours the instrumental phase tends to wander slightly because of ambient thermal effects. This drifting (with a 24 hour period) ultimately contributes more to the uncertainty in Δh and $\Delta\delta$ than do the random phase fluctuations due to either the atmosphere on clear days or receiver noise. To reduce this effect, calibration sources were observed briefly every 2 hours during each run. From these it was found that the instrumental phase drifted by as much as 0.5 rad total during some runs. With the aid of frequent calibrations, the drift in phase was removed, with a remaining uncertainty of about 0.2 rad.

Another important source of error arises because the calibrator, being a continuum source, is observed through both sidebands of the interferometer, whereas the H_2O maser line is observed through only one sideband. Because of this, the line source has an additional contribution to its fringe phase equal to $\omega_{IF}\Delta\tau$, where ω_{IF} is the IF angular frequency and $\Delta\tau$ is the residual unbalance in signal delays to the correlators from the two antennas. For the present observations, the uncertainty in this quantity is 0.1 rad. This is an uncertainty in the constant of fringe phase for the unknown. For an observation of about 12 hours' duration, this constant does not affect the determination of Δh in the least-squares fit to equation (1). If the declination is at least 40°, it also has little effect on the derived $\Delta\delta$. However, for low declinations, the hour angle independent term is important, and this constant phase error has a significant effect on the derived $\Delta\delta$.

For the Hat Creek interferometer, the maximum east-west baseline gives $b_1 \approx b_3 \approx 0$ and $b_2 \approx 305$ m, whereas the maximum diagonal baseline gives $b_1 \approx 119$ m, $b_2 \approx 140$ m, and $b_3 \approx 152$ m. As can be seen from equation (1), high-declination source positions are best determined from an east-west baseline. The maximum sensitivity to $\Delta\delta$ then occurs at large hour angles where the elevation is low. The long-run observations were made during the period 1975 November to 1976 March during excellent weather conditions, and there was no evidence for systematic errors due to inadequate correction for refraction at low elevations. Figure 1 shows a typical fit obtained for W51.

b) Transit Measurements

The Δh and $\Delta\delta$ were determined, respectively, from a 300 m east-west and a 200 m north-south baseline. For a nearly east-west baseline ($b_1 \approx b_3 \approx 0$), the average phase near transit is, from equation (1),

$$\bar{\phi} = \frac{2\pi}{\lambda}\left[-b_2 \cos\delta\,\Delta h + (b_1 \sin\delta - b_3 \cos\delta)\Delta\delta + \Delta b_1 \cos\delta + \Delta b_3 \sin\delta\right] + \phi_{\rm inst}\,, \quad (2)$$

where

$$\bar{\phi} = \frac{1}{h}\int_{-h/2}^{h/2} \phi(h')dh'\,. \quad (3)$$

The instrumental phase, $\phi_{\rm inst}$, is determined by measuring $\bar{\phi}$ for a nearby quasar. Instrumental phase

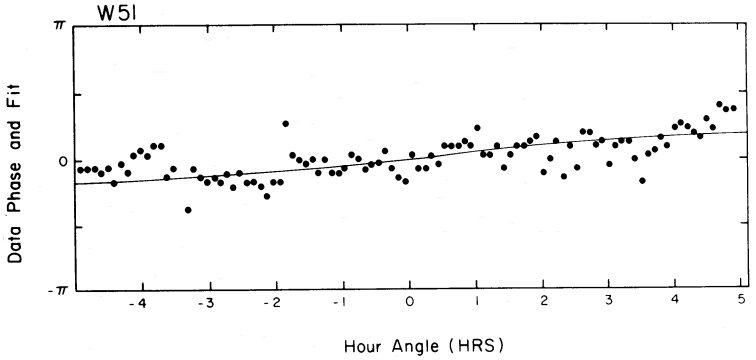

FIG. 1.—A typical absolute position fit obtained for 5 minute averages of a single 15 kHz channel at a velocity of 63.2 km s^{-1} in W51.

drifts are eliminated by measuring the quasar before and after the transit of the H_2O maser source. The increment Δh is then computed from the first term in equation (2). The remaining terms are error terms. Since $b_2 \approx 300$ m, whereas b_1 and $b_3 \lesssim 10^{-2}$ m, $\Delta\delta \approx 10^{-5}$ rad, and Δb_1 and $\Delta b_3 \approx 3 \times 10^{-3}$ m, these small terms contribute negligible error. For a nearly N-S baseline ($b_2 \approx 0$), equation (1) becomes

$$\bar{\phi} = \frac{2\pi}{\lambda}[(-b_1 \sin\delta + b_3 \cos\delta)\Delta\delta - b_2 \cos\delta\, \Delta h + \Delta b_1 \cos\delta + \Delta b_3 \sin\delta] + \phi_{\text{inst}} . \quad (4)$$

Here b_1 and $b_3 \approx 150$ m, while $b_2 \approx 10^{-2}$ m; so the error terms are again negligible. The principal source of error in these transit measurements is from the term $\omega_{\text{IF}}\Delta\tau$ as discussed earlier.

As a check on the accuracy of these methods, the positions of one set of quasars were measured by using another set of quasars as the baseline and instrumental phase calibrators. Mean errors were 0".3. The transit measurements were made in 1976 October and November, and, within the estimated errors (specified in Table 1), agreed with the earlier long observations.

III. RESULTS

The measured positions and probable errors are summarized in Table 1. The results for each source are discussed briefly below.

a) ON 1

We have already discussed (Baudry, Forster, and Welch 1974) the radio continuum and maser sources in ON 1. The H_2O position measurements made at Hat Creek in 1976 March improve our earlier (1973) results. The 10 km s^{-1} feature lies on the northeastern edge (Fig. 2*b*) of the radio source mapped at 8 GHz by Lo (1975). The same picture is obtained when our H_2O position is compared with the radio continuum position and size derived by Winnberg, Habing, and Goss (1973) and by Harris (1974). Hefele, Wacker, and Weinberger (1977) report a 3 σ upper limit of 6.5 Jy for any 10.7 μm emission from this source.

b) ON 2

ON 2 is an obscured region at a kinematic distance of about 5.5 kpc (Reifenstein *et al.* 1970). It contains three small continuum sources G75.84+0.4, G75.78+0.34, and G75.77+0.34 (Matthews *et al.* 1973; Turner *et al.* 1974; Harris 1976), along with time-variable OH and H_2O maser sources. From 1975 November to 1976 February the main water-vapor emission was detected around 4 km s^{-1}. The 4.4 and -1.2 km s^{-1} features (Fig. 3*a*) were found to vary in less than $\sim$1.5 months. They are situated on the edge of the compact component G75.78+0.34 (Fig. 3*b*) which is nearly coincident with the 1665 and 1667 MHz OH position derived by Hardebeck and Wilson (1971). Hefele *et al.* report a 3 σ upper limit for 10.7 μm emission from this source of 3.4 Jy. Note that the physical parameters of G75.78+0.34 and the associated H_2O source are very similar to those of ON 1. The weaker H_2O feature at -11.6 km s^{-1} lies in the outskirts of the diffuse region G75.77+0.34, not shown in Figure 3*b*.

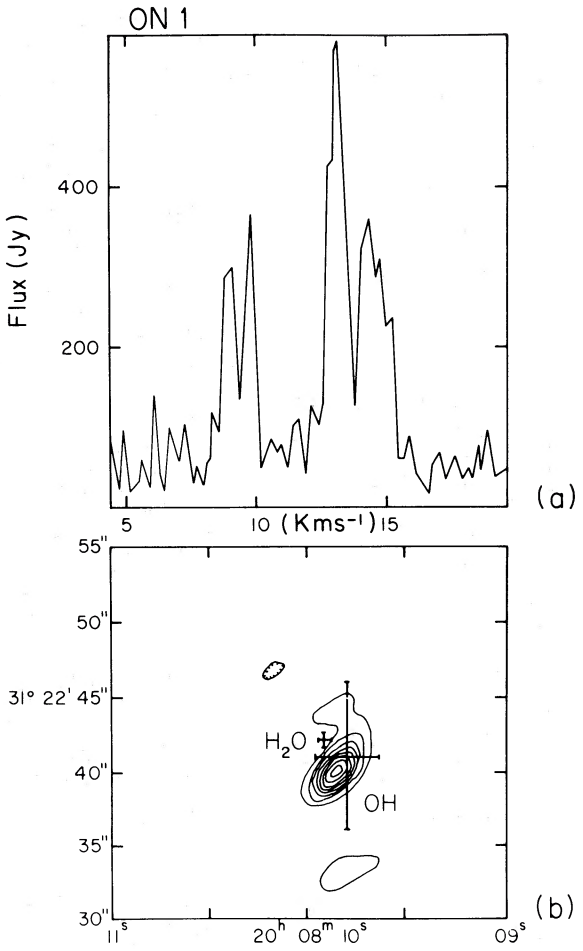

FIG. 2.—(*a*) Amplitude spectrum for a 3 hour coherent integration on the H_2O source in ON 1. (*b*) Positions of H_2O and OH maser sources superposed on an 8 GHz continuum map (Lo 1975).

c) NGC 7538

This is a diffuse nebula with incomplete shell-like structure at optical and radio wavelengths (Israel, Habing, and de Jong 1973). The presence of two O stars within the nebula suggests that it is more evolved than is the compact component at the southeastern edge of the ionized region. The radio continuum and infrared maps have resolved this component into three main subsources (Martin 1973; Wynn-Williams, Becklin, and Neugebauer 1974), one of which, component B of size $\sim$1" (Harris and Scott 1976), coincides with the 1665 and 1720 MHz OH sources (Wynn-Williams, Werner, and Wilson 1974).

TABLE 1
SOURCE POSITIONS

Source	Object	Radial Velocity (km/sec)	R A(1950)	Dec. (1950)	Reference and Remarks
ON 1	H_2O	13.5	$20^h08^m09^s.91\pm.03$	31°22'42".3± 0.4	This paper
	OH(1665)	13/16	09 .80±.50	41 .0±15.0	Hardebeck (1972)
	H II(8GHz)		09 .85±.02	40 .0± 0.25	Lo (1975)
ON 2	H_2O	4.4, -1.2	$20^h19^m51^s.79\pm.03$	37°17'01".2± 0.5	This paper
		-11.6	48 .90±.03	15 52 .10±0.75	This paper
	OH(1665/1667)	-4	51 .90±.40	17 03 .0±15.0	Hardebeck and Wilson (1971)
	H II G75.84 + 0.40(5GHz)		47 .40±.04	21 30 .2± 0.7	Matthews *et al.* (1973)
	G75.78 + 0.34(8GHz)		52 .00±.02	17 02 .0± 0.25	Lo (1975)
	G75.77 + 0.34(5GHz)		49 .99±.04	16 16 .0± 0.9	Matthews *et al.* (1973)
W51	H_2O	55.0	$19^h21^m26^s.195\pm.016$	14°24'43".6± 0.4	This paper
	OH(1665)	56.2/62.0	26 .3 ±0.2	35 ± 3.0	Wynn-Williams *et al.* (1974*a*)
			26 .3 ±0.4	39 ± 3.0	Raimond and Eliasson (1969)
	H II(15GHz)		26 .25± .02	41 .3± 0.4	Scott (1977)
VYCMA	H_2O	14.6	$07^h20^m54^s.66\pm .02$	-25°40'12".2± 1.0	
	OH		55 .0 ±0.6	11 ± 5.0	Eliasson and Bartlett (1969)
	optical		54 .603±.03	11.91± 0.3	
ORION	H_2O				
		7.6	$05^h32^m46^s.59\pm.02$	-05°24'31".5±0.5	This paper
		10.8	47 .58	09 .3	
		14.8	46 .92	22 .6	
		16.8	47 .00	23 .5	
		26	46 .33	33 .0	
SAGB2	H_2O	43.6/53.6	$17^h44^m10^s.03\pm.03$	-28°21'16".3±1.0	This paper
	H II(8GHz)		10 .6±0.1	16 ±3.0	Balick and Sanders (1974)
W75S	H_2O	0.6	$20^h37^m14^s.13\pm.03$	42°12'12".4± .4	This paper
	OH(1665)	-0.2/+5.6	14 .7±0.4	12 09 .0±3.0	Raimond and Eliasson (1969)
	IRS 1	(2/20μ)	10 .2±1.0	12 09 ± 10	Wynn-Williams *et al.* (1974*b*)
NGC 7538	H_2O	-54.4	$23^h11^m36^s.11\pm.05$	61°10'29".6±0.5	This paper
		-61.2	36 .47±.05	11 49 .4±0.5	This paper
	OH(1665)	-57.9/-59.1	36 .1±0.7	10 29 .0±5.0	Wynn-Williams *et al.* (1974*a*)
		-54.3/-56.5	36 .5±0.4	11 49 .0±3.0	Wynn-Williams *et al.* (1974*a*)
	OH(1720)	-57.2/-56.5	36 .8±0.4	11 49 .0±3.0	Wynn-Williams *et al.* (1974*a*)
	NGC 7538 (15GHz)		36 .68±.02	11 46 .64±0.1	Harris and Scott (1976)
	IRS 1(20μ) Nebula Center		36 .7±0.5	11 49 ±5.0	Wynn-Williams *et al.* (1974*b*)

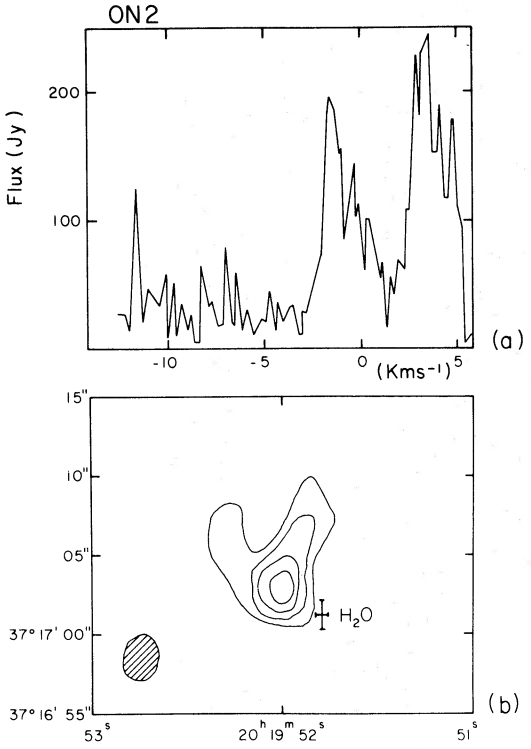

FIG. 3.—(*a*) Amplitude spectrum for a 4 hour coherent integration on the H_2O emission from ON 2. (*b*) Position of the H_2O maser source superposed on a 5 GHz contour map of the compact component G75.78+0.34 (Harris 1976).

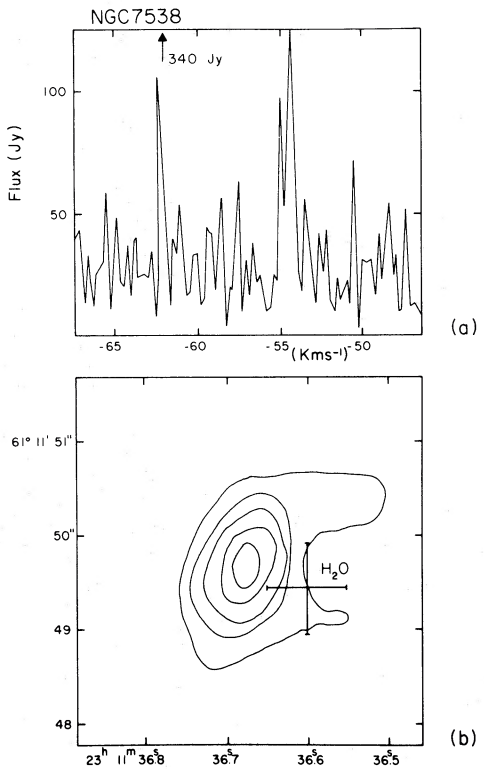

FIG. 4.—(*a*) Amplitude spectrum for a 12 hour coherent integration of the H_2O source at position $23^h11^m36^s.1$, 61°10′29″.6 in NGC 7538. The arrow marks the position of the only feature in the H_2O spectrum obtained in a 12 hour coherent integration at a position $23^h11^m36^s.47$, 61°11′49″.4. (*b*) Position of the northern H_2O source superposed on a 15 GHz contour map (Harris and Scott 1976).

The water-vapor emission from NGC 7538 is complex and time-variable. Strong features appear in the range -50 to -61 km s^{-1} (e.g., Baudry and Welch 1974), while weaker features appear at higher negative velocities (Genzel and Downes 1976). Our position analysis shows that the strongest feature, -54.4 km s^{-1} at the time of observation (Fig. 4*a*), lies $\sim$1″.5 south of component B and coincides within the errors with the southern OH source localized by Wynn-Williams, Werner, and Wilson (1974). The upper limit for 20 μm emission from this source is 300 Jy (Wynn-Williams, Becklin, and Neugebauer 1974).

A second, slightly fainter feature at -61 km s^{-1} lies to one side of the compact component B, as shown in Figure 4*b*. Significant maser emission from this direction first appeared in early 1976 and has been reported by Genzel and Downes (1976). IRS 1, a compact source smaller than 3″ with a strong silicate absorption feature in its spectrum, coincides with component B within its positional uncertainty of about 4″ (Wynn-Williams, Becklin, and Neugebauer 1974).

d) W51

This is a giant H II region situated at a distance of about 7 kpc (Wilson *et al.* 1970) in the Sagittarius major arm. The main H_2O features arise in the range 50–70 km s^{-1}. High-velocity features have also been reported in W51 (Goss *et al.* 1976; Morris 1976). The main features are strongly time-variable, as shown by Sullivan (1973). Figure 5*a* shows the spectrum measured in 1975 November with the 15 kHz filters. The H_2O features all lie within 2″ to one side (Fig. 5*b*) of a compact ionized region recently mapped at 15 GHz with the Cambridge 5 km telescope (Scott 1978). OH interferometer measurements (Wynn-Williams, Werner, and Wilson 1974) localize the 1665 MHz maser to the south of the main H_2O positions given above. This is directly confirmed by Mader *et al.* (1975), who found an OH/H_2O relative separation of $\Delta\delta = -7''$. No discrete infrared source with flux greater than 25 Jy at 20 μm or 0.1 Jy at 2.2 μm is observed in the direction of the H_2O maser (Wynn-Williams, Becklin, and Neugebauer 1974).

e) W75 S(OH)

W75 is a complex region at a distance of 1.5 kpc (Reifenstein *et al.* 1970) exhibiting emission from many molecules, infrared sources, and small H II regions. We found strong H_2O emission coming from very close to the OH position determined by Raimond and Eliasson (1969). Figure 6 shows the source position relative to infrared objects in the region. The OH/H_2O emission also lies at the edge of an HCN emission

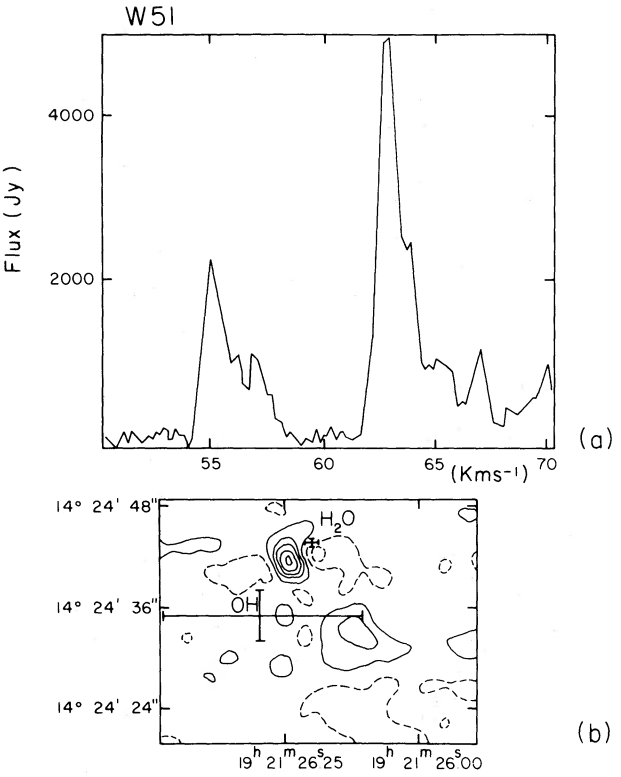

FIG. 5.—(*a*) Amplitude spectrum for a 2 hour integration on the H_2O source in W51. (*b*) Positions of H_2O and OH maser sources superposed on a part of the continuum map at 15 GHz made with the Cambridge 5 km telescope (Scott 1978). Note compression of the declination scale.

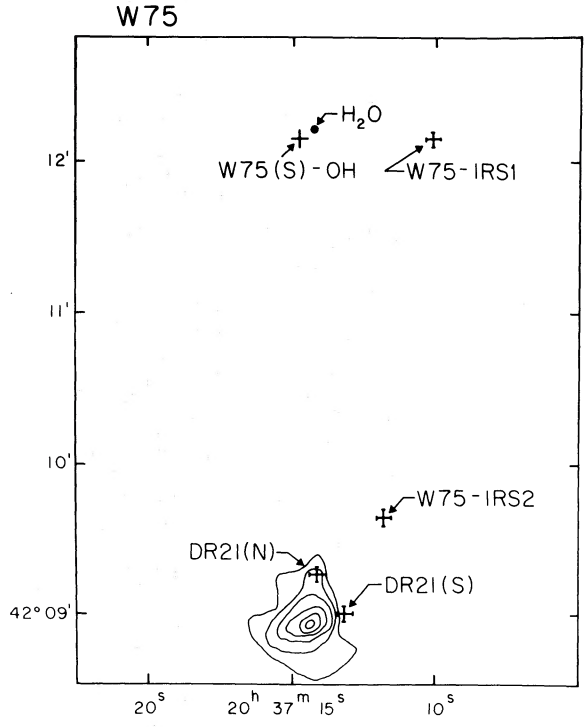

FIG. 6.—Position of the H_2O maser in W75 with respect to the OH maser, IR sources, and the radio continuum source DR 21. Weak IR emission is at the OH/H_2O location.

peak which is centered on IRS 1 (Morris *et al.* 1974). No continuum radiation greater than 15 mJy at 5 GHz is found near the OH/H_2O masers (Harris 1974). Weak, extended infrared radiation is found approximately centered at the maser position (Wynn-Williams, Becklin, and Neugebauer 1974).

f) *VY Canis Majoris*

Our recently determined position is substantially more accurate than the value reported by Baudry, Forster, and Welch (1974). It is very close to that of the stellar image. Both the strongest feature at 14.6 km s^{-1} and the weaker ones at 17 km s^{-1} and -3.6 km s^{-1} are in the same location within 0".1. Note that the separation in right ascension of the H_2O source and the optical image is slightly greater than the sum of the estimated errors. Unfortunately, at this low declination, the foreshortening of the baseline and the atmospheric refraction effects give rise to a larger uncertainty in the measurement of declination.

g) *Sagittarius B2*

Water-vapor emission from this region is quite variable and comes from several different locations (Morris 1976; Goss *et al.* 1976; Genzel, Downes, and Bieging 1976). At the time of our observation, the most intense spectral peak was at 48.6 km s^{-1}, and our quoted position is for all features in a 10 km s^{-1} interval centered at 48.6 km s^{-1}. This corresponds to maser group H_2O (2) of Genzel *et al.* and, indeed, is close to their value of $\alpha(1950) = 17^h44^m10^s.4 \pm 0^s.2$, $\delta(1950) = -28°21'21'' \pm 3''$ for the group. This position is at the edge of the strongest continuum source—No. 4 on the list of Martin and Downes (1972) and the northern source of Balick and Sanders (1974), a small H II region of about 12" diameter. The H II position given in Table 1 is that of Balick and Sanders (1974). Strong far-infrared radiation comes from Sgr B2, but nothing is observed at 2–20 μm (Becklin *et al.* 1977), both probably because the color temperature of the radiation is low and because the near-infrared optical depth to the source is quite large. The OH maser emission also comes from various different locations (e.g., Bieging 1976) that are about 1' south of our H_2O position.

h) *Orion*

This complex H II region is located at a distance of 0.5 kpc (Mezger and Höglund 1967) and contains at least five compact IR sources (Rieke, Low, and Kleinmann 1973), one of which has a position coincident with one of the H_2O masers within the errors. Although the IR sources and the H_2O masers are spread over roughly the same area in the nebula, separations of at least 4" (about 10^{16} cm) appear to be the rule; the one positional coincidence is probably a

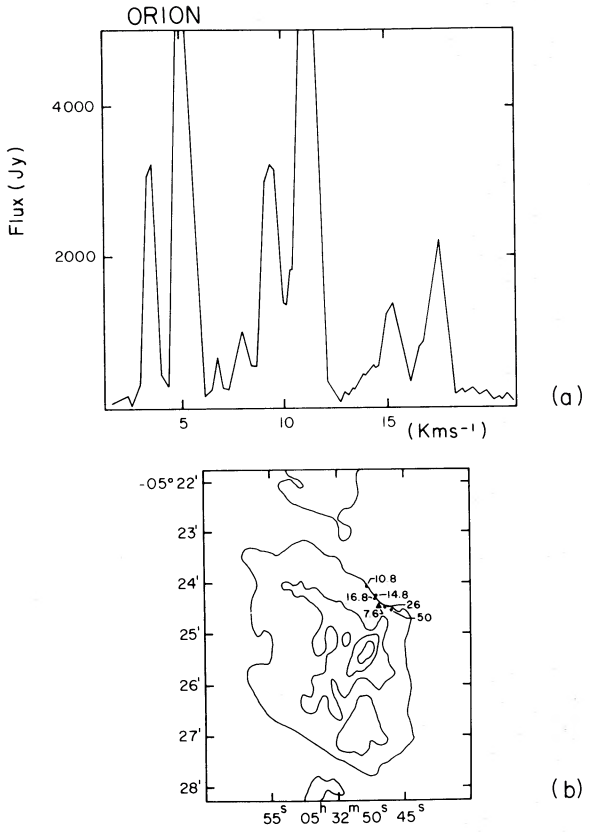

FIG. 7.—(*a*) Amplitude spectrum for 1 hour coherent integration on the H_2O source in Orion. (*b*) H_2O sources and the Kleinmann-Low nebula center (▲) superposed on a 5 GHz continuum map (Martin and Gull 1976). The -50 km s^{-1} H_2O feature was taken from Goss *et al.* (1976).

projection effect. Maser emission in the range -10 km s^{-1} to 30 km s^{-1} and the -50 km s^{-1} feature of Goss *et al.* (1976) are located (Fig. 7*b*) along the edge of the 5 GHz continuum emission (Martin and Gull 1976) which arises in an H II region bounded by a dense cloud of molecular hydrogen (Kutner and Thaddeus 1971; Zuckerman 1973). OH masers are also found in this region (Raimond and Eliasson 1969), and these appear closer to the compact IR sources within the Kleinmann-Low nebula than do the H_2O sources.

IV. DISCUSSION

For 10 strong H_2O masers in eight regions, we have measured precise positions with accuracies of the order of 0".5. Locating these objects with respect to nearby OH masers, IR sources, and compact H II regions gives information about these dense regions where stars are thought to be forming. At the present time, the positions of the small H II regions are the most accurately known; therefore, comparison of the H_2O maser positions with these objects is the most informative. The OH masers and IR source positions are still uncertain within a few arcsec, and the relation of the H_2O masers to these objects remains less certain, except in the few cases where differential H_2O/OH positions have been obtained. Nevertheless, it is useful to summarize the (possible) coincidences of these small objects, including the sources in W3 (continuum), W3(OH), and CRL 2591 for which accurate interferometer positions have been reported elsewhere (Forster, Welch, and Wright 1977; Wynn-Williams *et al.* 1977). Among the 13 H_2O maser sources (or groups of spots), (*a*) no infrared point sources are coincident in eight cases; (*b*) OH masers may be coincident in six cases, although, in those regions where the OH positions are most accurately known [e.g., W3(OH)], they generally are displaced from the H_2O; and (*c*) H_2O masers are adjacent to compact H II regions in five cases.

There is only one example of an H_2O maser at the edge of a small H II region where there is also an infrared source coincident within observational error: the northern source in NGC 7538 (at the southern edge of the nebula). As discussed by Genzel and Downes (1976), this may be indeed a young massive star within an opaque cocoon of dust, with maser emission which arises in the dense region between the ionization and shock fronts surrounding the star. Figure 4*b* shows the H_2O emission just at the edge of the ionized region. The observed infrared radiation is presumed to come from this dense shell.

On the other hand, this simple symmetric picture does not fit the other four cases in which a maser is found at the edge of a compact H II region. The main difficulty is that no infrared emission is observed toward these sources. The dense shell of dust and gas surrounding the ionized region in the cocoon star models, such as those described by Davidson and Harwit (1967), Kahn (1974), Yorke and Krugel (1977), and Cochran and Ostriker (1977), has high infrared luminosity. Maser action requires $T \gtrsim 300$ K, if collisional processes are important, and molecular hydrogen densities in the range 10^7–10^{11} cm^{-3} in order to have high gains and yet avoid collisional quenching. These conditions are found ahead of the ionization front within the shell of the cocoon stars. Taking as a typical shell density $n_{H_2} = 10^8$ cm^{-3} (Cochran and Ostriker 1977), we derive, assuming for the dust $\tau \approx 4 \times 10^{-23} n_{H_2} L$ in the 10–20 μm range,[1] an optical depth greater than 1 for shells thicker than only $L = 2.6 \times 10^{14}$ cm. Hence the near-infrared luminosity of the shell is known from its angular diameter and from the dust temperature. The compact H II region W51, for example, has a diameter of $\sim$0".5, 5×10^{16} cm at 7 kpc distance; if it were surrounded by a dust shell at 300 K, it would produce a flux of about 2400 Jy at 20 μm. The upper limit of Wynn-Williams, Becklin, and Neugebauer (1974) for this direction is 25 Jy. Even lower limits are found for

[1] The infrared optical depth of a layer of dust of thickness L is $\tau = n_g \pi r^2 Q_{ext} L$. With the mass of dust 1% that of the gas and with a mean grain radius r of 0.2 μm, the number density of grains is $n_g = 5 \times 10^{-13} n_{H_2}$. The extinction efficiency factor $Q_{ext} L \approx 0.06$ for a mixture of ice, graphite, and silicate grains at 10–20 μm wavelength.

ON 1 and ON 2 (Hefele *et al.*) at 10 μm. It is more likely that the water maser emission arises in an independent, dense, but small fragment at the edge of the H II region. The maser may be pumped by the collision with the expanding H II region, but it is in the separate fragment. In addition to the infrared argument above, the appearance of the continuum maps of Figures 2, 3, and 5 supports this picture. In each case, the lowest continuum contour suggests that the H II region has collided with a denser region where the maser is located and into which the ionizing radiation has not penetrated but around which this radiation is spilling. Figure 4 suggests a similar picture for NGC 7538 as well.

We are suggesting that the H_2O maser emission generally arises in separate dense fragments rather than in the shells surrounding massive stars. Conditions for the maser action require H_2 densities in the range 10^7–10^{11} cm^{-3} and path lengths of 10^{14}–10^{16} cm. The masses of such fragments may be substantial. A sphere of 10^{16} cm diameter and 10^9 cm^{-3} density has a mass of 1 $M_\odot$. However, such an object at a temperature of 300 K would be very luminous in the infrared. Since infrared point sources frequently do not coincide with the masers, it is likely that the dense ($n_{H_2} \approx 10^9$ cm^{-3}) fragments are smaller than 1 $M_\odot$ and generally irregular in shape, and that there are many of them. In this case, maser emission may be seen along the long axis of the fragment, and the apparent size of the maser, as measured by VLBI techniques, would be close to the true transverse size of the elongated structure. Excitation of the maser emission may be due to collisions between fragments. This would explain the lack of correlation between velocity and position in relative H_2O maps. The frequent appearance of the masers at the edge of small H II regions may be due to excitation of the fragment by collision with the expanding ionized gas. Finally, the masers may be giving us the first glimpse of the fragmentation process in the dense molecular clouds.

It is a pleasure to acknowledge the assistance of John Dreher, Douglas Thornton, and Wilson Hoffman in the development and calibration of the instrument; the staff at Hat Creek for their assistance with observations; and valuable conversations with Charles Townes, Joe Silk, David Cudaback, and Jill Tarter. Paul Scott kindly provided the W51 15 GHz map in advance of publication. The work was supported by the NSF under grant AST 75-13511.

REFERENCES

Balick, B., and Sanders, R. H. 1974, *Ap. J.*, **192**, 325.
Baudry, A., Forster, J. R., and Welch, W. J. 1974, *Astr. Ap.*, **36**, 217.
Baudry, A., and Welch, W. J. 1974, *Astr. Ap.*, **31**, 471.
Becklin, E. E., Matthews, K., Neugebauer, G., and Wynn-Williams, C. G. 1977, *Astr. Ap.*, **55**, 19.
Bieging, J. H. 1976, *Astr. Ap.*, **51**, 289.
Cochran, W. D., and Ostriker, J. P. 1977, *Ap. J.*, **211**, 392.
Davidson, K., and Harwit, M. 1967, *Ap. J.*, **148**, 443.
Dieter, H. H., Welch, W. J., and Wright, M. C. H. 1978, in preparation.
Eliasson, B., and Bartlett, J. F. 1969, *Ap. J.* (*Letters*), **155**, L79.
Elsmore, B., and Ryle, M. 1976, *M.N.R.A.S.*, **174**, 411.
Forster, J. R., Welch, W. J., and Wright, M. C. H. 1977, *Ap. J.* (*Letters*), **215**, L121.
Genzel, R., and Downes, D. 1976, *Nature*, **262**, 564.
Genzel, R., Downes, D., and Bieging, J. 1976, *M.N.R.A.S.*, **177**, 101P.
Goss, W. M., Knowles, S. H., Balister, M., Batchelor, R. A., and Wellington, K. J. 1976, *M.N.R.A.S.*, **174**, 541.
Hardebeck, E. G. 1972, *Ap. J.*, **172**, 583.
Hardebeck, E. G., and Wilson, W. J. 1971, *Ap. J.* (*Letters*), **169**, L123.
Harris, S. 1974, *M.N.R.A.S.*, **166**, 29P.
———. 1976, *M.N.R.A.S.*, **174**, 1.
Harris, S., and Scott, P. F. 1976, *M.N.R.A.S.*, **175**, 371.
Hefele, H., Wacker, W., and Weinberger, R. 1977, *Astr. Ap.*, **56**, 407.
Israel, F. P., Habing, H. J., and de Jong, T. 1973, *Astr. Ap.*, **27**, 143.
Kahn, F. D. 1974, *Astr. Ap.*, **37**, 149.
Kutner, M., and Thaddeus, P. 1971, *Ap. J.* (*Letters*), **168**, L67.
Lo, K. Y. 1975, Ph.D. thesis, M.I.T.
Mader, G. L., Johnston, K. J., Moran, J. M., Knowles, S. H., Mango, S. A., Schwartz, P. R., and Waltman, W. B. 1975, *Ap. J.* (*Letters*), **200**, L111.
Martin, A. H. M. 1973, *M.N.R.A.S.*, **163**, 141.
Martin, A. H. M., and Downes, D. 1972, *Ap. Letters*, **11**, 219.
Martin, A. H. M., and Gull, S. F. 1976, *M.N.R.A.S.*, **175**, 235.
Matthews, H. E., Goss, W. M., Winnberg, A., and Habing, H. J. 1973, *Astr. Ap.*, **29**, 309.
Mezger, P. G., and Höglund, B. 1967, *Ap. J.*, **147**, 490.
Morris, M. 1976, *Ap. J.*, **210**, 100.
Morris, M., Palmer, P., Turner, B. E., and Zuckerman, B. 1974, *Ap. J.*, **191**, 349.
Raimond, E., and Eliasson, B. 1969, *Ap. J.*, **155**, 817.
Reifenstein, E. C., Wilson, T. L., Burke, B. F., Mezger, P. G., and Altenhof, W. J. 1970, *Astr. Ap.*, **4**, 357.
Rieke, G. H., Low, F. J., and Kleinmann, D. E. 1973, *Ap. J.* (*Letters*), **186**, L7.
Scott, P. F. 1978, in preparation.
Sullivan, W. T., III. 1973, *Ap. J. Suppl.*, **25**, 393.
Turner, B. E., Balick, B., Cudaback, D. D., Heiles, C., and Boyle, R. J. 1974, *Ap. J.*, **194**, 279.
Welch, W. J., Forster, J. R., Dreher, J., Hoffman, W., Thornton, D. D., and Wright, M. C. H. 1977, *Astr. Ap.*, **59**, 385.
Wilson, T. L., Mezger, P. G., Gardner, F. F., and Milne, D. K. 1970, *Ap. Letters*, **5**, 99.
Winnberg, A., Habing, H. J., and Goss, W. M. 1973, *Nature Phys. Sci.*, **243**, 78.
Wynn-Williams, C. G., Becklin, E. E., Forster, J. R., Matthews, K., Neugebauer, G., Welch, W. J., and Wright, M. C. H. 1977, *Ap. J.* (*Letters*), **211**, L89.
Wynn-Williams, C. G., Becklin, E. E., and Neugebauer, G. 1974, *Ap. J.*, **187**, 473 (cited as 1974*b* in Table 1).
Wynn-Williams, C. G., Werner, M. W., and Wilson, W. J. 1974, *Ap. J.*, **187**, 41 (cited as 1974*a* in Table 1).
Yorke, H. W., and Krugel, E. 1977, *Astr. Ap.*, **54**, 183.
Zuckerman, B. 1973, *Ap. J.*, **183**, 863.

ALAIN BAUDRY: Observatoire de l'Université de Bordeaux, 33270 Floirac, France

J. R. FORSTER, W. J. WELCH, and M. C. H. WRIGHT: Radio Astronomy Laboratory, University of California, Berkeley, CA 94720